

Tidal imprint on the gravitational signal emitted by BH-NS coalescing binaries

V Ferrari¹, L Gualtieri¹ and F Pannarale¹

¹ Dipartimento di Fisica “G.Marconi”, Sapienza Università di Roma
and Sezione INFN ROMA1, piazzale Aldo Moro 2, I-00185 Roma, Italy

Abstract. We compute the gravitational signal emitted in the latest phases of the coalescence of a binary system composed of a stellar mass black hole and a neutron star, prior to merging. Tidal interactions are taken into account by means of the affine model approach, in which the neutron star is viewed as a deformable ellipsoid. We compare the orbital and the tidal contributions to the signal, assuming that the star moves in a region where, although very close to the black hole, it has not been disrupted yet. We show that during the last revolutions the star is a non-spherical oscillating object. Indeed, the non-radial oscillations of the star are excited and produce a multiple peak structure in the emitted signal, due to mode coupling, and to the coupling between orbital motion and tidal interaction. This model could be a useful tool to provide reliable initial conditions for numerical relativity simulations of merging processes.

PACS numbers: 04.40.Dg; 97.10.Sj

1. Introduction

The evolution of compact binary systems is of considerable interest in astrophysics. The coalescence of these binaries may be schematically divided in three stages [1],[2]. The first and longest one (10^{8-10} years [3]) is the quasi-equilibrium inspiral phase, during which the two companions move in orbits which slowly shrink and circularize as energy is carried away by gravitational radiation. The orbits become unstable at the innermost stable circular orbit (ISCO), where the plunge and merger phase starts. The last stage of the evolution is the ringdown phase, during which the object resulting from the merging process oscillates in its proper modes, emitting gravitational waves at the corresponding frequencies until it settles down to equilibrium.

During the past three decades, theorists have been modelling various kinds of double compact objects. Stellar mass black hole (BH) - neutron star (NS) coalescing binaries, in particular, are believed to be among the most promising sources of gravitational waves that could be detected by interferometers working above 10 Hz (see for example [3],[4] and references therein) and thus accurate templates are needed to extract signals from the background noise and to interpret possible measurements. BH-NS mergers, moreover, have also been invoked along with NS-NS mergers as possible engines of short gamma-ray bursts (see [5] for example). These two reasons have therefore lead to a significant effort in modelling such coalescing systems. Unfortunately, BH-NS as well as BH-BH binaries (as opposed to NS-NS binaries [6]) have not been observed yet, therefore it is not currently possible to infer their

properties from observational data. Thus, in modelling the behaviour of these binaries and in making predictions about them, one has to rely on binary evolution and population synthesis models [7],[8].

Several approaches addressing different issues have been employed to study coalescing binaries. Post-Newtonian (PN) studies of compact binaries ([9] and references therein), for example, typically approximate the constituents of the binary as point sources. PN expansions may not converge sufficiently rapidly in the strong-field region and thus are indicated for the inspiral phase. Other approaches go under the name of “hydro without hydro” methods and use “snapshots” generated by quasi-equilibrium codes [2],[10] in order to include finite-size effects in the inspiral phase but without solving explicitly hydrodynamic equations. Finite size-effects are connected to tidal interactions between the binary’s constituents. These interactions are present well before the final phases of the coalescence and have been studied in the literature using various approaches and addressing several issues. We refer the reader to [11] for an overview on the literature. We mention that there are two important classes of numerical techniques that deal with such effects and which mainly address the merger and ringdown phases of compact binary evolution: 3-D Smoothed Particle Hydrodynamics (SPH) codes and grid-based codes. Both techniques have been employed in a Newtonian and in a general relativistic framework (see [12],[13] for SPH and [14], [15] for grid-based codes). It should be mentioned that the ringdown phase can also be studied using perturbative approaches [16], providing the initial oscillation amplitude of the object resulting from the coalescence is known from merger’s simulations.

In this paper we focus on BH-NS tidal interactions and on the gravitational waves emitted during the late phases of the inspiral prior to the merger, keeping in mind that, just before the ISCO, full-GR grid based codes should step-in to integrate the merger. In the phase we are interested in, gravitational waves are essentially generated by two mechanisms: the time variation of the system’s quadrupole moment caused by orbital motion and the time variation of the NS’s quadrupole moment due to its deformation triggered by tidal interactions with the BH. We address the problem by using the affine model approach introduced, in Newtonian gravity, by Carter and Luminet in [17], and adopted in [11] to compute the gravitational signal emitted by white dwarf (WD)-BH binaries. Since the orbital separation becomes very small in the case of BH-NS coalescence, we cannot neglect general relativistic effects on the tidal interaction and on the orbital motion. In order to take the former effects into account, we use the generalization of the affine model developed in [18] by Marck and Luminet, and we include gravitational radiation reaction.

We study the motion and deformation of a NS with mass $M_* = 1.4 M_\odot$ during the coalescence with a BH with mass $M_{BH} = 10 M_\odot$, and we compute the gravitational signal due to both the orbital motion and the stellar deformation. In a recent study on the formation and evolution of binary populations, based on population synthesis calculations [8], the contribution of BH-BH, BH-NS and NS-NS binaries to the detection rates of ground-based gravitational wave detectors has been estimated, and the chirp mass, mass ratio and component mass distributions of these binaries have been determined. According to the reference model adopted by the authors, for BH-NS binaries the chirp mass and the mass ratio are expected to be $\sim (2.5 \div 3) M_\odot$ and $q < 0.2$, respectively; M_* peaks at $\sim 1.35 M_\odot$ and M_{BH} is found in the wide range $\sim (3 \div 11) M_\odot$ with increasing contribution at the higher mass end. Our choice for M_* and M_{BH} is compatible with these results (in our case $M_{chirp} \simeq 3 M_\odot$ and $q = 0.14$).

We point out that recent numerical simulations [19] have assumed $M_{BH} = 3.2 M_\odot$ and $M_{BH} = 4 M_\odot$ for the BH and $M_* = 1.4 M_\odot$ for the NS, values marginally compatible with the results just discussed.

Our integrations start at $r_0 \sim 100 (M_{BH} + M_*)$; as the star approaches the BH, tidal interactions trigger oscillations in the NS and cause the emission of gravitational waves, at its proper oscillation frequencies, which add up to the binary's orbital gravitational emission.

As mentioned above, BH-NS coalescence has recently been studied in numerical simulations performed in full general relativity [13], [19]. In these works the initial data are determined by solving the Hamiltonian constraint at small values of the orbital separation: $\sim 11 M_{BH}$ in [13], $\sim 6 (M_{BH} + M_*)$ in [19] (we also mention the simulation of head-on BH-NS collision in [20], with initial separation $\sim 60 M_\odot = 12 M_{BH}$). Therefore, in the present state of art of fully relativistic numerical simulations, the oscillations that the star undergoes in the previous phase of the coalescence are not taken into account. In this respect, the results of our integrations may be useful in obtaining initial data for fully general relativistic simulations.

The paper is organized as follows. In Section 2 we describe our approach, in Section 3 we present the results of our numerical simulations, and in Section 4 we draw our conclusions.

2. The Model

To describe the evolution of the binary system we work in the *tidal approximation*, i.e. we assume that:

- $M_{BH} \gg M_*$ (we remind that M_{BH} is the hole's mass and M_* the star's mass)
- the star's deformations do not influence its orbital motion.

In this approximation, we can view the black hole as a central object and the star as an extended test-body moving in the Schwarzschild metric

$$ds^2 = - \left(1 - \frac{2M_{BH}}{r}\right) dt^2 + \left(1 - \frac{2M_{BH}}{r}\right)^{-1} dr^2 + r^2 (d\theta^2 + \sin^2 \theta d\phi^2). \quad (1)$$

Furthermore, the tidal approximation allows us to treat the star's orbital motion and its deformations separately. We neglect the perturbation that the oscillating star induces on the BH.

Hereafter we will assume geometrical units $c = G = 1$, and we will denote \mathcal{O}_P the coordinate frame $\{t, r, \theta, \phi\}$ (centred in the black hole) in which (1) is expressed.

2.1. Orbital Motion and Tidal Tensor

We determine the orbital motion of the NS around the BH using formulae which take into account gravitational radiation reaction up to 1PN order (i.e. the quadrupole formalism, see for instance [21]). They are accurate in the slow motion and weak field limit, which is satisfied as long as we do not consider the evolution of the system close to merger. As discussed in [13], the orbital motion of astrophysically relevant BH-NS

binaries has been circularized in the initial phase of the coalescence, therefore it can be considered as a circular motion with time-dependent radius:

$$r(t) = r_0 \left(1 - \frac{t}{t_{coal}} \right)^{1/4} \quad (2)$$

where r_0 is the orbital separation at $t = 0$ and

$$t_{coal} \equiv \frac{5r_0^4}{256M_*M_{BH}^2} \quad (3)$$

is the coalescence time. The equations for the orbital motion are

$$\frac{d\tau}{dt} = \sqrt{1 - \frac{3M_{BH}}{r(t)}} \quad (4)$$

$$\frac{d\phi}{dt} = \sqrt{\frac{M_{BH}}{r(t)^3}} \quad (5)$$

where τ is the proper time. The energy per unit mass

$$E = \left(1 - \frac{2M_{BH}}{r} \right) \frac{dt}{d\tau} \quad (6)$$

and the orbital angular momentum per unit mass

$$\ell = r^2 \frac{d\phi}{d\tau} \quad (7)$$

are constant in the geodesic motion, but they change in the actual NS motion due to gravitational wave emission. In the frame \mathcal{O}_P previously defined, let the 4-vector $\xi_P \equiv (\xi^t, \xi^r, \xi^\theta, \xi^\phi)$ indicate the separation between a generic fluid cell of the star and its centre of mass. Moreover, let \mathcal{O}_* be the reference frame centered in the star's centre of mass and parallel transported along geodesic motion. Let $\{\mathbf{e}_{(0)}, \dots, \mathbf{e}_{(3)}\}$ be the 4-vectors of an orthonormal tetrad associated to \mathcal{O}_* , which undergoes parallel transport along the orbit (as long as gravitational radiation reaction can be neglected, and the motion is geodesic). In this and in the following section, we will use Greek indexes ($\alpha = 0, \dots, 3$) for tensor components and Latin indexes ($i = 1, \dots, 3$) for space tetrad components.

The geodesic deviation equation can be expressed in this frame as [22]

$$\frac{d^2 \xi_*^i}{d\tau^2} + C^i_{\ j} \xi_*^j = 0 \quad (8)$$

where the displacement 3-vector $\vec{\xi}_*(\tau)$ is given by

$$\xi_*^i = e_{\mu}^{(i)} \xi_P^\mu \quad (9)$$

and C_{ij} , called *tidal tensor*, is given by the projection of the Riemann tensor $R_{\alpha\beta\gamma\delta}$ on the tetrad $\mathbf{e}_{(\mu)}$ as follows:

$$C_{ij} = R_{\alpha\beta\gamma\delta} e_{(0)}^\alpha e_{(i)}^\beta e_{(0)}^\gamma e_{(j)}^\delta. \quad (10)$$

In the Schwarzschild metric the Riemann tensor and the Weyl tensor $C_{\alpha\beta\gamma\delta}$ coincide, therefore we can write

$$C_{ij} = C_{\alpha\beta\gamma\delta} e_{(0)}^\alpha e_{(i)}^\beta e_{(0)}^\gamma e_{(j)}^\delta. \quad (11)$$

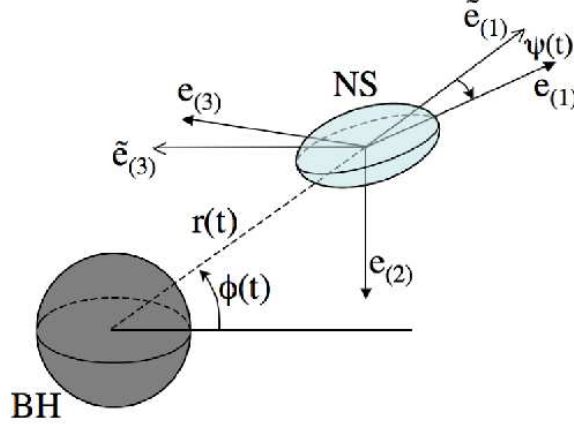


Figure 1. A pictorial representation of ψ and of the tetrad defined by (12).

The tetrad associated to the \mathcal{O}_* frame (introduced in [18]) is

$$\begin{aligned}
 e_{(0)}^\mu &= \dot{t}\delta_0^\mu + \dot{r}\delta_1^\mu + \dot{\phi}\delta_3^\mu \\
 e_{(1)}^\mu &= \tilde{e}_{(1)}^\mu \cos \psi - \tilde{e}_{(3)}^\mu \sin \psi \\
 e_{(2)}^\mu &= \frac{1}{r}\delta_2^\mu \\
 e_{(3)}^\mu &= \tilde{e}_{(1)}^\mu \sin \psi + \tilde{e}_{(3)}^\mu \cos \psi
 \end{aligned} \tag{12}$$

where a dot indicates differentiation respect to the proper time τ , δ_ν^μ is the Kronecker delta, $\tilde{e}_{(1)}^\mu$ and $\tilde{e}_{(3)}^\mu$ are given by

$$\begin{aligned}
 \tilde{e}_{(1)}^\mu &= \frac{r}{(r^2 + \ell^2)^{1/2}} \left(\frac{\dot{r}}{1 - \frac{2M_{BH}}{r}} \delta_0^\mu + E \delta_1^\mu \right) \\
 \tilde{e}_{(3)}^\mu &= \frac{\ell}{(r^2 + \ell^2)^{1/2}} \left(\frac{E}{1 - \frac{2M_{BH}}{r}} \delta_0^\mu + \dot{r} \delta_1^\mu \right) + \frac{\sqrt{r^2 + \ell^2}}{r^2} \delta_3^\mu.
 \end{aligned} \tag{13}$$

The tetrad (12) has been defined as follows. $\mathbf{e}_{(0)}$ coincides with the 4-velocity of the star's centre of mass, the spatial part of $\mathbf{e}_{(2)}$ is perpendicular to the orbital plane, and the spatial parts of $\mathbf{e}_{(1)}$ and $\mathbf{e}_{(3)}$ lie in the orbital plane. The four vectors $\mathbf{e}_{(0)}, \dots, \mathbf{e}_{(3)}$ are parallel transported in the orbital motion (as long as gravitational radiation reaction can be neglected). The vectors $\mathbf{e}_{(1)}$, $\mathbf{e}_{(3)}$ are related to the vectors $\tilde{\mathbf{e}}_{(1)}$, $\tilde{\mathbf{e}}_{(3)}$ (13) (where $\tilde{\mathbf{e}}_{(1)}$ is directed towards the BH, and $\tilde{\mathbf{e}}_{(3)}$ is orthogonal to $\tilde{\mathbf{e}}_{(1)}$) by a rotation of an angle ψ in the orbital plane (Figure 1). The angle $\psi(\tau)$ is governed by the equation

$$\frac{d\psi}{d\tau} = \frac{E\ell}{r^2 + \ell^2}. \tag{14}$$

For the orbits we are considering, equations (4), (6), (7) and (14) yield

$$\frac{d\psi}{dt} = \sqrt{\frac{M_{BH}}{r(t)^3} \left(1 - \frac{3M_{BH}}{r(t)} \right)}. \tag{15}$$

Replacing (12) in (10) we find the explicit expressions of the tidal tensor:

$$\begin{aligned}
C_{11} &= \frac{M_{BH}}{r^3} \left(1 - 3 \frac{r^2 + \ell^2}{r^2} \cos^2 \psi \right) \\
C_{22} &= \frac{M_{BH}}{r^3} \left(1 + 3 \frac{\ell^2}{r^2} \right) \\
C_{33} &= \frac{M_{BH}}{r^3} \left(1 - 3 \frac{r^2 + \ell^2}{r^2} \sin^2 \psi \right) \\
C_{13} = C_{31} &= -3 \frac{r^2 + \ell^2}{r^5} M_{BH} \sin \psi \cos \psi.
\end{aligned} \tag{16}$$

2.2. Affine Model Equations

To describe the tidal interaction between the neutron star and the black hole we use the affine model developed by Carter and Luminet [17] and generalized by Marck and Luminet to the Schwarzschild black hole case [18]. In this model we assume that the BH is left unperturbed by the tidal interaction and that the star is deformed maintaining an ellipsoidal shape. Furthermore we describe the structure and dynamics of stellar deformations with Newtonian physics. All quantities are evaluated in the frame \mathcal{O}_* , corresponding to the tetrad (12).

We assume that the star is composed by a perfect fluid with a polytropic equation of state

$$P = K\rho^\gamma \tag{17}$$

where P, ρ are the pressure and the mass density of the fluid, respectively. We also assume that the stellar mass M_* is constant, i.e. that there is no mass transfer. We indicate the stellar radius in the spherical equilibrium configuration with \hat{R} ; hereafter the ‘hat’ ($\hat{}$) will denote quantities computed for the unperturbed star.

This model is named “affine” because it relies in the assumption that (in the frame \mathcal{O}_*) the star maintains an ellipsoidal configuration while it interacts with the black hole; therefore, the position 3-vector $\vec{\xi}_*$ of a fluid cell, defined in (9), is given at any instant of proper time by

$$\xi_*^i = q_j^i \hat{\xi}^j \tag{18}$$

where $q_j^i = q_j^i(\tau)$ is a 3×3 matrix which does not depend on space coordinates, and $\hat{\xi}^j$ are the coordinates of the cell’s position 3-vector in an initial known configuration. For example, a spherical equilibrium configuration is given by $q_j^i = \delta_j^i$ and $\dot{q}_j^i = 0 \ \forall i, j$.

The affine model [17] allows a Lagrangian description of the stellar deformation dynamics in terms of the variables q_j^i which leads to the following set of second order ordinary differential equations:

$$\ddot{q}_j^i = -C_k^i q_j^k + \frac{\hat{\Pi}}{\hat{\mathcal{M}}} \left[\|q\|^{1-\gamma} (q^{-T})^i{}_j - \frac{3}{2} \int_0^\infty du \frac{[(S + uI)^{-1}]_n^i}{\Delta} q_j^n \right] \tag{19}$$

where the C_j^i ’s are given by (16), $\hat{\Pi}$ is the volume integral of the local pressure calculated in the initial configuration, i.e.

$$\hat{\Pi} = \int P d\hat{V}, \tag{20}$$

$\widehat{\mathcal{M}}$ is the star's scalar quadrupole moment in the initial configuration

$$\widehat{\mathcal{M}} = \frac{1}{3} \int \widehat{\xi}^i \widehat{\xi}^i dM_*, \quad (21)$$

$||q||$ indicates the determinant of the deformation matrix, q^{-T} its inverse and transposed, S is a matrix defined as

$$S_{ij} \equiv q_{ik} q_{jk}, \quad (22)$$

I is the identity and

$$\Delta \equiv \sqrt{||S + uI||}. \quad (23)$$

The physical meaning of equations (19) is the following: the first term gives the star's tidal interaction with the Schwarzschild black hole; the second and third terms describe, respectively, the internal energy of the stellar fluid and its self-gravity.

By diagonalizing S , one obtains the squares of the principal axes of the stellar ellipsoid, i.e.

$$S_{ij} = \begin{pmatrix} a_1^2 & 0 & 0 \\ 0 & a_2^2 & 0 \\ 0 & 0 & a_3^2 \end{pmatrix}. \quad (24)$$

Expressions for a_1, a_2 and a_3 in terms of the elements of q can be found in [17]. The directions corresponding to a_i , i.e. the principal axes of the ellipsoid, are different both from the directions of $\mathbf{e}_{(i)}$ and from the directions of $\tilde{\mathbf{e}}_{(i)}$; however, the a_1 direction, where we find the largest deformations, is close to the direction of $\tilde{\mathbf{e}}_{(1)}$, which points towards the black hole.

2.3. Quadrupole Moment of the Binary

We compute the gravitational signal emitted by the binary system by using the quadrupole formalism (see for instance [21]), according to which

$$\begin{cases} h_{TT}^{\mu 0} = 0 \\ h_{TT}^{ik}(t, d) = \frac{2G}{c^4 d} \left[\frac{d^2}{dt^2} Q_{TT}^{ik} \left(t - \frac{d}{c} \right) \right] \end{cases} \quad (25)$$

($\mu = 0, \dots, 3$, $i, k = 1, \dots, 3$) where d is the distance of the observer from the source and Q_{TT}^{ik} is the quadrupole moment of the system projected in the TT-gauge (transverse-traceless gauge), that is

$$Q_{TT}^{ij} = \mathcal{P}^{ijlm} Q^{lm} \quad (26)$$

\mathcal{P}^{ijlm} being a tensor projector appropriately defined.

For the system we are considering, the quadrupole moment is given by

$$\begin{aligned} Q^{ik}(t) &\equiv \frac{1}{c^2} \int_V T^{00}(t, x^j) x^i x^k d^3x = \\ &= \int_V \rho_C(t, \xi_C^j) (X_C^i + \xi_C^i) (X_C^k + \xi_C^k) d^3\xi_C, \end{aligned} \quad (27)$$

where V is the volume of the star, the C denotes Cartesian coordinates associated to the black hole's reference frame, ρ_C is the mass-density of the star, X_C^i are the spatial (Cartesian) coordinates of the star's centre of mass position vector with respect to the black hole singularity and the ξ_C^i 's are the ξ_*^i 's (see equation (18)) expressed in Cartesian coordinates associated to the BH (for more details we refer to Appendix

A). The integral is calculated only on the star's volume because the black hole is spherically symmetric for all t 's. By expanding such integral we have

$$\begin{aligned} Q^{ik}(t) = & \int_V \rho_C(t, \xi_C^j) X_C^i(t) X_C^k(t) d^3 \xi_C + \int_V \rho_C(t, \xi_C^j) \xi_C^i \xi_C^k d^3 \xi_C + \\ & + X_C^i(t) \int_V \rho_C(t, \xi_C^j) \xi_C^k d^3 \xi_C + X_C^k(t) \int_V \rho_C(t, \xi_C^j) \xi_C^i d^3 \xi_C. \end{aligned} \quad (28)$$

The first term is the standard quadrupole moment associated to the star's orbital motion around the black hole

$$Q_{orb}^{ik}(t) = X_C^i(t) X_C^k(t) \int_V \rho_C(t, \xi_C^j) d^3 \xi_C = M_* X_C^i(t) X_C^k(t); \quad (29)$$

the second term is due to the star's deformation. To evaluate it we notice that the relations $d^3 \xi_* = ||q|| d\hat{\xi}$ and $\rho = \hat{\rho} ||q||^{-1}$, which follow from (18), take the following form in Cartesian coordinates

$$d^3 \xi_C = ||q_C|| d\hat{\xi}_C \quad \text{and} \quad \rho_C = \hat{\rho}_C \cdot ||q_C||^{-1}. \quad (30)$$

This is true because an affine relation of the form $\xi_C^i = q_C^i{}_j(t) \hat{\xi}_C^j$ holds in Cartesian coordinates; this may be easily proved by applying a coordinate transformation to (18) (see Appendix A). Thus

$$\begin{aligned} Q_{def}^{ik}(t) = & \int_V \rho_C(t, \xi_C^j) \xi_C^i \xi_C^k d^3 \xi_C = \\ & = q_C^i{}_l(t) q_C^k{}_m(t) \int_V \hat{\rho}_C(t, \hat{\xi}_C^j) \hat{\xi}_C^l \hat{\xi}_C^m d^3 \hat{\xi}_C = \\ & = q_C^i{}_l(t) q_C^k{}_m(t) \int_V \hat{\xi}_C^l \hat{\xi}_C^m dM = \hat{\mathcal{M}} S_C^i{}_k(t), \end{aligned} \quad (31)$$

where we have used $\hat{\rho}_C = dM_*/d\hat{V}_C$ and we have defined $S_C^i{}_j \equiv q_C^i{}_k q_C^j{}_k$ in analogy with (22).

The last two integrals in (27) vanish since for every fluid element of coordinates $\hat{\xi}_C^i = (x^i, y^i, z^i)$ in the unperturbed configuration there exists one with coordinates $(-x^i, -y^i, -z^i)$.

In conclusion the quadrupole moment of the system consists of two contributions, the orbital one Q_{orb}^{ik} (29) and the one due to the tidal interaction Q_{def}^{ik} (31):

$$Q_{orb}^{ik}(t) = M_* X_C^i(t) X_C^k(t) \quad (32)$$

$$Q_{def}^{ik}(t) = \hat{\mathcal{M}} S_C^i{}_k(t). \quad (33)$$

Notice that $\hat{\mathcal{M}}$ acts as an effective mass for the deformations.

2.4. Chirp Waveform

To calculate the orbital contribution to the gravitational wave it is possible to use analytical expressions obtained from equations (32). Starting from (2) one can find that the amplitude and phase of the orbital signal are given by [21]:

$$h(t) = \frac{4M_* M_{BH}}{dr_0} \left(1 - \frac{t}{t_{coal}}\right)^{-1/4} \quad (34)$$

$$\Phi(t) = -2 \left[\frac{t_{coal} - t}{5M_*^{3/5} M_{BH}^{2/5}} \right]^{5/8} + \Phi_0. \quad (35)$$

This gives the well known chirp waveform which is typical of coalescing point masses. Notice that $M_*^{3/5} M_{BH}^{2/5}$ coincides with the chirp mass $M_{chirp} \equiv \mu^{3/5} M_{Tot}^{2/5}$ in the limit $M_* \ll M_{BH}$. Here $M_{Tot} = M_{BH} + M_*$.

3. Results for BH-NS Coalescence

We shall now discuss our results for the coalescence of a binary system composed of a black hole of mass $M_{BH} = 10 M_\odot$ ($R_S \simeq 29.5$ km) and a neutron star of mass $M_* = 1.4 M_\odot$. The NS's equilibrium radius is $\hat{R} = 15.7$ km and the adiabatic index is $\gamma = 5/3$. For further discussions, the values of two of the star's non-radial oscillation mode frequencies will be useful: the fundamental mode is $\nu_f \simeq 1605$ Hz, while the first pressure mode is $\nu_{p1} \simeq 3538$ Hz [23]. Finally, we remind the reader that the principal equations of the model are (2)-(5), (15) and (19).

3.1. Influence of the Initial Orbital Separation on the Integrations

In order to numerically integrate equations (4), (5), (15) and (19), we set initial conditions for the deformation matrix (q) and its first derivative with respect to proper time (\dot{q}) at the initial orbital separation r_0 . The best way to proceed is to seek for an r_0 such that it is reasonable to assume that the NS is in spherical equilibrium, that is we must look for an r_0 which allows us to set $q_j^i = \delta_j^i$ and $\dot{q}_j^i = 0$ (at $t = 0$). Keeping this in mind, we perform integrations starting with different values of r_0 and we look at the NS oblateness in the orbital plane which is defined as

$$\varepsilon_{Orb} \equiv 2 \frac{a_1 - a_3}{a_1 + a_3}. \quad (36)$$

In Figure 2 we compare ε_{Orb} obtained with four choices of r_0 (i.e. $25 M_{Tot}$, $33 M_{Tot}$, $65 M_{Tot}$ and $92 M_{Tot}$). As we see, ε_{Orb} oscillates and the amplitude of the oscillations converges as r_0 increases; the cases $r_0 = 25 M_{Tot}$ and $r_0 = 33 M_{Tot}$ indicate that a choice of the initial orbital separation incompatible with a spherical equilibrium configuration for the NS induces unphysical (and hence undesired) oscillations that one must accurately avoid. This clearly shows that it is fundamental to choose the initial conditions appropriately. If we choose $r_0 \sim 92 M_{Tot}$, we can be confident that unphysical effects are removed and we see that, as it orbits around the BH, the NS behaves as an *oscillating object* with an increasingly non-spherical shape.

On the basis of the analysis just described, we may finally set the parameters for a long integration of the BH-NS inspiral. We decide to start our full integration at $r_0 = 92 M_{Tot} = 1550$ km with the NS in spherical equilibrium. We end our integration at $r_{end} = 4 M_{Tot} = 67$ km. At this distance the behaviour of the principal axes of the stellar ellipsoid is still quite controlled, as we show in Figures 3 (left panel) and 6 (left panel). However, it is worth stressing that our stellar model is a very simple polytropic model with no crust. The distance from the black hole at which the star would be destroyed depends on the inner structure and on the crust structure, thus our results are only indicative in this respect. However, it is interesting to mention that if we push the integration beyond the critical radius $r_{crit} \simeq 4 M_{Tot} = 67$ km, where $a_1/\hat{R} = 1.5$, a_1 grows to such an extent that the numerical integration runs out of control. Notice that the ISCO radius for a test particle is $6 M_{Tot} = 101$ km, which is larger than the critical radius we find.

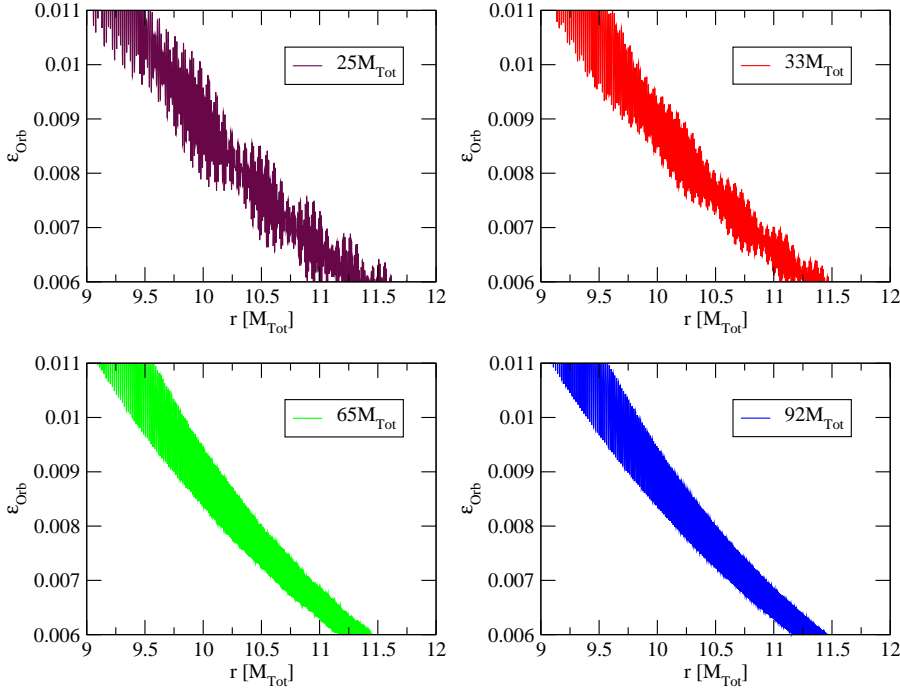


Figure 2. The oblateness in the orbital plane (ϵ_{Orb}) is plotted as a function of the BH-NS separation r for $r_0 = \{25, 33, 65, 92\}M_{Tot}$ ($M_{Tot} \simeq 16.84$ km). The oscillations converge as r_0 increases.

The data regarding the gravitational emission due to orbital motion (the chirp) are stored starting from $r \sim 450$ km: this corresponds to a chirp frequency of $\nu_{orb}^{GW} \simeq 40$ Hz, which is roughly the lower cut-off frequency of ground-based interferometers.

3.2. Complete Integration

We will first analyse the data obtained as the binary reduces its orbital separation from $r \simeq 1550$ km to $r \sim 6 M_{Tot} \simeq 101$ km, which corresponds to the ISCO radius for a test particle. It takes about 846s and about 4000 revolutions for this to happen; the initial and final orbital periods are, respectively, 333 ms and 5.5 ms.

Let us start by seeing what happens to the principal axes of the star during the inspiral (Figure 3 left panel). As expected the axis that points towards the BH singularity (a_1) grows as r diminishes. On the other hand, the values of the other two axes decrease: the neutron star tends to assume a *cigar-like* configuration ($a_1 > a_2, a_3$). When the NS reaches $\sim 6M_{Tot}$, $\epsilon_{Orb} \sim 0.05$. Therefore, when the NS is at a distance $r \simeq 6 M_{tot}$ from the black hole it is a *non-spherical oscillating* object.

Figure 3 (right panel) shows the strain amplitude $|h_+(\nu) + ih_-(\nu)|\sqrt{\nu}$ of the deformation contribution to the gravitational wave emitted by the binary system as the BH-NS separation evolves from ~ 1550 km to ~ 101 km; we label the peaks indicating their physical origin. The first peak we find can be traced back to the first addend in eq. (19): this term couples the stellar deformation to the orbital motion by means of

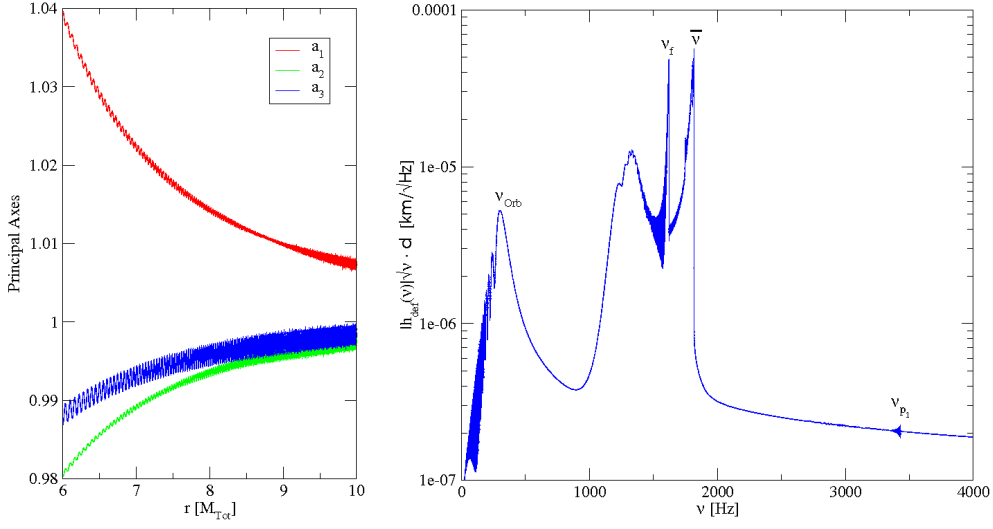


Figure 3. Axes of the stellar ellipsoid as functions of the BH-NS orbital separation r up to $r = 6 M_{Tot} \sim 101$ km (left) and corresponding strain amplitude of the deformation contribution to the gravitational wave (right). The strain amplitude is defined as $|h_+(\nu) + ih_-(\nu)|\sqrt{\nu}$ and it is multiplied by the distance d of the binary from the observer. Recall that a_1 points towards the BH singularity. All axes are normalized to their spherical equilibrium value $\hat{a}_i = \hat{R}$.

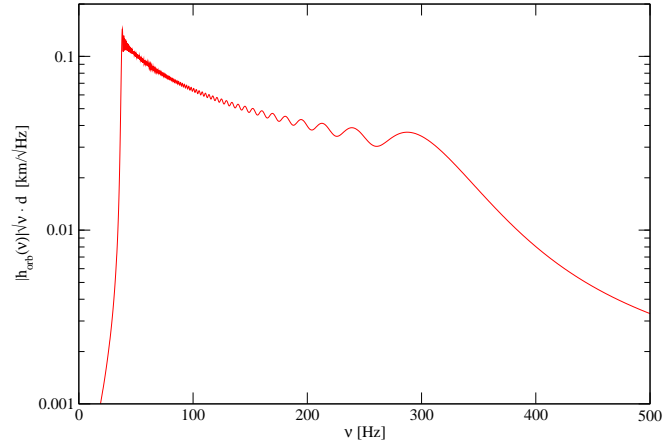


Figure 4. Strain amplitude of the orbital contribution to the gravitational wave emitted while r reduces from ~ 450 km to ~ 101 km.

the tidal tensor C_{ij} , which depends on the orbital separation $r(t)$; therefore it carries the information on the orbital evolution. For this reason, the frequencies of the chirp (Figure 4) are found also in the Fourier transform of the deformation signal.

At a different frequency range (above 1 KHz) we see that the gravitational wave generated by the tidal deformation carries information about the stellar non-radial oscillation modes. We recognize, in fact, the peaks corresponding to the frequencies ν_f and ν_{p_1} . The origin of the peak we label with $\bar{\nu}$ will be discussed below. The shape of these structures is determined by relativistic effects. When the star is at infinity with respect to the black hole, proper time and coordinate time do not differ ($d\tau/dt = 1$) and thus the modes contribute to the gravitational emission at the frequencies at which the star oscillates when it is perturbed from its spherical equilibrium configuration. As the orbital distance reduces, $d\tau/dt$ (4) diminishes and as a consequence the mode frequencies are redshifted in terms of coordinate time. In other words, the frequency at which a mode contributes to the wave is $\nu_i d\tau/dt$ (where i stands for f or p_1 in our case) and this value decreases during the inspiral. Moreover, the star departs from its spherical equilibrium configuration as it moves closer to the black hole and this changes its non-radial oscillation frequencies. According to this discussion, we expect the right edge of a peak to be given by the value of the frequency of the mode for the spherical NS multiplied by the factor $d\tau/dt$ calculated for r equal to 1550 km (r 's value when we start producing data) and this is indeed the case (Figure 3, right panel).

To gain deeper insight on the shape of the strain amplitude (Figure 3, right panel) of the gravitational wave generated by the stellar deformations, in particular on the peak labeled with $\bar{\nu}$, and on the “hump” that lies between ν_{orb} and ν_f , we compare it to the strain amplitudes obtained by considering subsets of the data. Figure 5 (to be compared with Figure 3, right panel) shows the results one obtains with this procedure. The upper left panel shows the strain amplitude obtained by the deformation signal emitted as the orbital separation reduces from 1550 km to 1308 km. The peak we indicated with “1” corresponds to “ ν_f ” in Figure 3 (right panel); in the same figure we indicated a peak with “ $\bar{\nu}$ ”, but here we can see that there are actually two contributions to it, indicated here as “2” and “3”. In the remaining three panels, as r varies from 389 km to 328 km, from 276 km to 233 km and from 169 km to 146 km, we are able to follow the three peaks spotted in the first panel (in the last panel “1” has actually been overtaken by “2”). These figures show the contributions to the signal due to particular parts of the inspiralling process, where the radial distance spans small ranges; therefore, they can roughly be considered as “snapshots” of the process at different values of r (corresponding to different values of ν_{orb} , which is the frequency of the gravitational wave generated by the orbital motion, i.e. twice the Keplerian frequency).

We see that the position of the peaks “1” and “3” does not significantly change as r and ν_{orb} change; their small shift is due to the dependence of the redshift factor $d\tau/dt$ on r . Conversely, the peak “2” is significantly shifted as the star approaches the black hole; indeed, $\nu_3 - \nu_2 \simeq \nu_{orb}$, and the splitting of the peak $\bar{\nu}$ in two can be interpreted as due to the coupling with the orbital frequency. We can state, as discussed above, that $\nu_1 = \nu_f$, that the third peak is some other oscillation mode of the star $\nu_3 = \bar{\nu}$, and that $\nu_2 = \bar{\nu} - \nu_{orb}$. A coupling of this kind is due to the first term in (19). The lower right panel indicates, moreover, that $\bar{\nu} - \nu_{orb}$, which spans lower values of the frequency as the star approaches the black hole, generates the “hump” between ν_{orb} and ν_f in Figure 3 (right panel).

The physical origin of the peak “3”, i.e. $\bar{\nu}$, is harder to determine. As we have

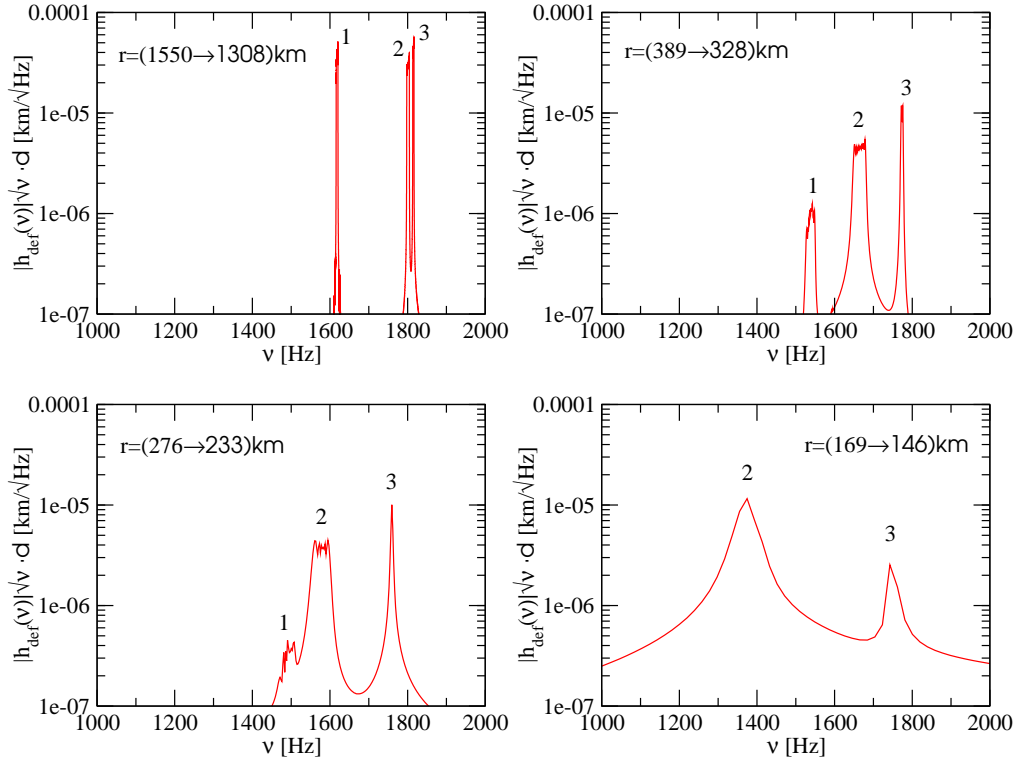


Figure 5. Strain amplitudes obtained from the deformation contribution to the gravitational wave emitted in the time intervals corresponding to an evolution of the binary system separation from 1550 km to 1308 km, from 389 km to 328 km, from 276 km to 233 km and from 169 km to 146 km. The panels should be compared to Figure 3 (right panel).

shown, it does not depend on the orbital motion of the star. Furthermore, it is not due to the cigar-like shape of the star, since it has the same location at $r \simeq 1500$ km, when the star is more or less spherical, and at $r \simeq 150$ km, when the deformation of the star is much larger. We concluded that this peak is probably due to the combination of the fundamental and the p_1 mode; indeed, $\bar{\nu} = \nu_{p_1} - \nu_f$. It could appear strange that this peak, due to a coupling between modes, is higher than the f -mode peak in Figure 3, but we remind the reader that in this figure we plot $h \cdot \sqrt{\nu}$; plotting h , the f -mode peak is the highest.

To conclude, we push our integrations as further as possible and consider the gravitational wave produced by the binary as its orbital radius r evolves beyond 101 km until $r_{crit} \simeq 4.567$ km. Figure 6 (left panel) shows the three principal axes of the stellar ellipsoid; a_1 in particular is about to start to grow uncontrolled. The NS is more cigar-like and its oblateness in the orbital plane is $\epsilon \sim 0.43$. The right panel shows the deformation strain amplitude. Comparing it with Figure 3 (right panel), one sees that it has become “noisier” and that the “ ν_{orb} ” structure grows in amplitude

(and occupies a wider frequency range) as r decreases because the oscillations become more violent, i.e. the coupling term in 19 becomes stronger.

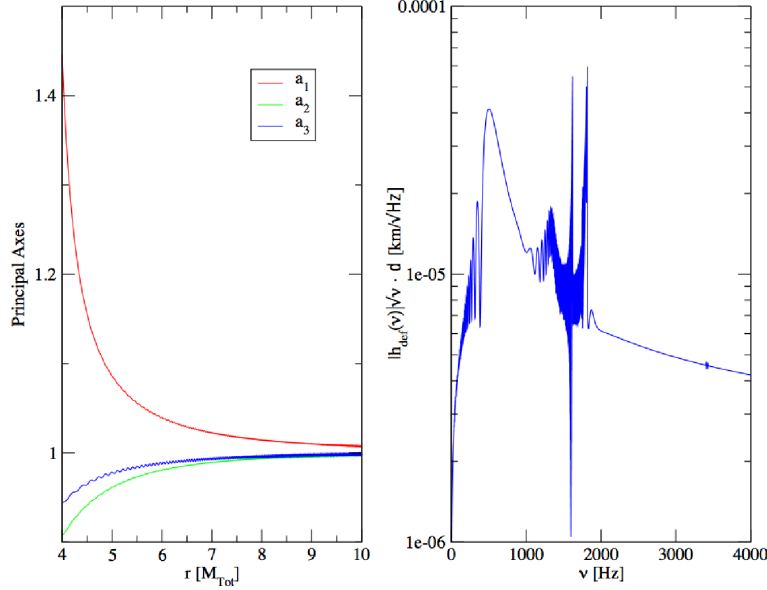


Figure 6. Neutron star’s principal axes versus the orbital radius r up to $r \sim 67$ km (left) and corresponding strain amplitude of the deformation contribution to the gravitational wave (right). The strain is defined as $|h_+(\nu) + ih_-(\nu)|\sqrt{\nu}$ and it is multiplied by the distance d of the observer from the binary. Recall that a_1 points towards the BH singularity. All axes are normalized to their spherical equilibrium value $\hat{a}_i = \hat{R}$.

4. Conclusions

In this paper we studied the tidal interactions that a NS undergoes during its last phases of circular inspiral around a Schwarzschild BH and we computed the gravitational signal emitted by this system. We assumed that the star is close to the BH, but moves in a region safe enough to prevent its tidal disruption; we also assumed that the oscillations induced by the tidal interactions do not affect the orbit of the NS. Tidal interactions in the binary have been taken into account by means of the affine model approach in which the NS is viewed as a deformable ellipsoid and no dynamical behaviour has been included for the black hole.

We analyzed in detail a binary system composed by a $1.4 M_{\odot}$ neutron star and a $10 M_{\odot}$ Schwarzschild black hole. We showed that the star is deformed during the inspiral and that its non-radial oscillation modes are excited: the NS reaches the ISCO as a *non-spherical oscillating object*. This result is important for numerical integrations of merging processes. In fact, it is in contrast with the spherical equilibrium initial conditions and/or the non-oscillating initial conditions that have often been adopted for the NS in grid based and Smoothed Particle Hydrodynamics integrations of BH-NS mergers. Assuming the star to be spherical and non-oscillating when it is close to the BH is erroneous and determines a loss of the physical processes concerning tidal

interactions that the system undergoes during the late inspiral phase of its coalescence. This model may thus be a useful tool to estimate more reliable initial conditions for numerical relativity simulations of merging processes.

We also showed that the tidal contribution to the gravitational wave (h_{def}) carries a signature of the NS's non-radial oscillation modes at frequencies which are different (i.e. higher) from the ones at which the orbital motion contributes (h_{orb}). This signature is present in the form of sharp peaks in the strain of h_{def} . The shape of such peaks is moreover affected by relativistic redshift effects.

Appendix A. Coordinate Changes

In section 2.3 we mentioned the need to express the displacement 3-vector $\vec{\xi}_*$ in Cartesian coordinates associated to the black hole singularity. We will briefly discuss how to perform these coordinate changes [24]. Bold characters shall indicate 4-vectors.

The tetrad $\mathbf{e}_{(\mu)}$ comoving with the star, corresponding to the frame \mathcal{O}_* and defined in (12), may be expressed in polar coordinates associated to the reference frame \mathcal{O}_P , centered in the BH singularity, as follows:

$$\begin{aligned}\mathbf{e}_{(0)} &\equiv (\dot{t}, \dot{r}, 0, \dot{\phi}) \\ \mathbf{e}_{(1)} &\equiv \left(\frac{r\dot{r}\cos\psi - \ell E \sin\psi}{AB}, \frac{rE\cos\psi - \ell\dot{r}\sin\psi}{B}, 0, -\frac{B\sin\psi}{r^2} \right) \\ \mathbf{e}_{(2)} &\equiv (0, 0, \frac{1}{r}, 0) \\ \mathbf{e}_{(3)} &\equiv \left(\frac{r\dot{r}\sin\psi + \ell E \cos\psi}{AB}, \frac{rE\sin\psi + \ell\dot{r}\cos\psi}{B}, 0, \frac{B\cos\psi}{r^2} \right)\end{aligned}\quad (\text{A.1})$$

where $A = A(r) \equiv 1 - 2M_{BH}/r$, $B = B(r, \ell) \equiv \sqrt{r^2 + \ell^2}$. The matrix Λ' relating the tetrad $\{\mathbf{e}_{(0)}, \mathbf{e}_{(1)}, \mathbf{e}_{(2)}, \mathbf{e}_{(3)}\}$ to the polar coordinate basis $\{\partial_t, \partial_r, \partial_\theta, \partial_\phi\}$ by

$$\mathbf{e}_{(\mu)} = \Lambda'^{\alpha}_{(\mu)} \partial_\alpha \quad (\alpha = t, r, \theta, \phi) \quad (\text{A.2})$$

is thus given by

$$\Lambda' \equiv \begin{pmatrix} \dot{t} & \frac{r\dot{r}\cos\psi - \ell E \sin\psi}{AB} & 0 & \frac{r\dot{r}\sin\psi + \ell E \cos\psi}{AB} \\ \dot{r} & \frac{rE\cos\psi - \ell\dot{r}\sin\psi}{B} & 0 & \frac{rE\sin\psi + \ell\dot{r}\cos\psi}{B} \\ 0 & 0 & \frac{1}{r} & 0 \\ \frac{\ell}{r^2} & -\frac{B\sin\psi}{r^2} & 0 & \frac{B\cos\psi}{r^2} \end{pmatrix}. \quad (\text{A.3})$$

The polar coordinate basis may then be related to the Cartesian coordinate basis $\{\partial_t, \partial_x, \partial_y, \partial_z\}$ centered in the BH singularity by

$$\partial_\alpha = \Lambda''^{\beta}_{\alpha} \partial_\beta \quad (\alpha = t, r, \theta, \phi; \beta = t, x, y, z), \quad (\text{A.4})$$

the matrix Λ'' being

$$\Lambda'' \equiv \begin{pmatrix} 1 & 0 & 0 & 0 \\ 0 & \sin\theta\cos\phi & r\cos\theta\cos\phi & -r\sin\theta\sin\phi \\ 0 & \sin\theta\sin\phi & r\cos\theta\sin\phi & r\sin\theta\cos\phi \\ 0 & \cos\theta & -r\sin\theta & 0 \end{pmatrix}. \quad (\text{A.5})$$

Having determined Λ' and Λ'' , the 4-vector ξ_C may be found at once from the 4-vector ξ_* (see (27)) by using

$$\xi_C = \Lambda'' \Lambda' \xi_*. \quad (\text{A.6})$$

- [1] Postnov K A and Yungelson L R 2006 *Living Rev. Relativity* **9**, 6.
- [2] Duez M D, Baumgarte T W and Shapiro S L 2001 *Phys. Rev.* **D63**, 084030.
- [3] Janka H T and Ruffert M, [arXiv:astro-ph/0101357](#);
Ruffert M and Janka H T 2001 *AIP Conf. Proc.* **662**, 193.
- [4] Coleman Miller M 2007 *AIP Conf. Proc.* **924**, 681.
- [5] Carter B 1992 *Astrophys. J.* **391**, L67 (1992);
Janka H T, Eberl T, Ruffert M and Fryer C L 1999 *Astrophys. J.* **527**, L39;
Coleman Miller M 2005 *Astrophys. J.* **626**, L41;
Rantsiou E, Kobayashi S, Laguna P and Rasio F A, [arXiv:astro-ph/0703599](#).
- [6] Thorsett S E and Chakrabarty D 1999 *Astrophys. J.* **512**, 288;
Burgay M, D'Amico N, Possenti A *et al.* 2003 *Nature* **426**, 531.
- [7] Nelemans G, Yungelson L R, and Portegies Zwart S F 2001 *Astron. & Astrophys.* **375**, 890.
- [8] Belczynski K, Taam R E, Kalogera V, Rasio F A, and Bulik T 2007 *Astrophys. J.* **662**, 504.
- [9] Blanchet L 2006 *Living Rev. Relativity* **9**, 4.
- [10] Sopuerta C F, Sperhake U and Laguna P 2006 *Class. Quant. Grav.* **23**, S579.
- [11] Casavieri C, Ferrari V, Stavridis A 2006 *Mon. Not. Roy. Astron. Soc.* **365**, 929.
- [12] Hernquist L 1993 *Astrophys. J.* **404**, 717;
Xing Z G, Centrella J M and McMillan S L W 1994 *Phys. Rev.* **D50**, 6247;
Lee W H and Kluzniak W 1999 *Astrophys. J.* **526**, 178;
Rasio F A and Shapiro S L 1999 *Class. Quant. Grav.* **16**, R1-R29;
Lee W H and Kluzniak W 1999 *Mon. Not. Roy. Astron. Soc.* **308**, 780;
Lee W H 2001 *Mon. Not. Roy. Astron. Soc.* **328**, 583.
- [13] Faber J A, Baumgarte T W, Shapiro S L, Taniguchi K and Rasio F A 2006 *Phys. Rev.* **D73**, 024012.
- [14] Ruffert M H, Janka H T and Schafer G 1996 *Astron. & Astrophys.* **311**, 532;
Ruffert M, Rampp M and Janka H T 1997 *Astron. & Astrophys.* **321**, 991.
- [15] Shibata M and Uryu K 2001 *Phys. Rev.* **D64**, 104017;
Tsokaros A A and Uryu K 2007 *Phys. Rev.* **D75**, 044026.
- [16] Berti E, Cardoso V, Will C M 2006 *Phys. Rev.* **D73**, 064030.
- [17] Carter B and Luminet J P 1982 *Nature* **296**, 211;
Carter B and Luminet J P 1983 *Astron. & Astrophys.* **121**, 97;
Carter and Luminet J P 1985 *Mon. Not. Roy. Astron. Soc.* **212**, 23;
Luminet J P and Carter B 1986 *Astrophys. J.* **61**, 219.
- [18] Marck J A 1983 *Proc. R. Soc. Lond.* **A385**, 431;
Marck J A 1983 *Phys. Lett.* **A97**, 140;
Luminet J P and Marck J A 1985 *Mon. Not. Roy. Astron. Soc.* **212**, 57.
- [19] Shibata M and Uryu K 2006 *Phys. Rev.* **D74**, 121503;
Shibata M and Uryu K 2007 *Class. Quant. Grav.* **24**, S125.
- [20] Loffler F, Rezzolla L and Ansorg M 2006 *Phys. Rev.* **D74**, 104018 (2006).
- [21] Misner C W, Thorne K S and Wheeler J A 1973, *Gravitation*, W H Freeman & C, New York.
- [22] Pirani F A E 1956 *Acta Phys. Polonica* **15**, 389.
- [23] Cox J P 1980 *Theory of stellar pulsation*, Princeton Un. Press, Princeton, N.J. .
- [24] Pannarale F 2006 *Master Thesis in Physics, University of Rome "La Sapienza"*, unpublished.